Mean flow scaling in a spanwise rotating channel

By X. Yang†, Z.-H. Xia‡, J. Lee¶, Y. Lv‖ AND J.-L. Yuan††

1. Motivation and objectives

Turbulence is often encountered in rotating frames of reference, e.g., over oceans, around windmills, in turbomachines, where the frames in question revolve with the earth and human-made rotating devices (Smirnov & Menter 2009; Arolla & Durbin 2013; Hsieh *et al.* 2016). The flows are responsible for transport of water vapor, generation of lift and drag, and mixing of fuel and oxidizer in the above contexts. Effects of these flows at practically relevant conditions are difficult to compute accurately due to the cost requirement (Choi & Moin 2012), and therefore engineers often have to rely on empirical relations (e.g., the law of the wall) to compute wall friction using velocity information at an off-wall location.

The law of the wall, also known as the universal logarithmic law of the wall, was proposed in the early 1930s by Theodor von Kármán and Ludwig Prandtl (Von Kármán 1930; Prandtl 1925). It asserts that the mean velocity increases linearly with the logarithm of the distance from the wall, i.e., $U^+ = 1/\kappa \log(y^+) + B$, where U is the mean flow velocity at a wall-normal distance y, the superscript + indicates normalization by wall units, κ is the von Kármán constant (Marusic *et al.* 2013; Nagib & Chauhan 2008), and B is another constant. Relating wall-shear stresses to velocities at off-wall locations, the law of the wall is useful for turbulence modeling in a non-rotating reference frame (Piomelli & Balaras 2002; Bose & Park 2018; Yang & Meneveau 2016), but its predictive power is partly lost if the flow is in a rotating device, e.g., in a spanwise rotating channel (Launder *et al.* 1987; Hamba 2006; Grundestam *et al.* 2008*b*).

Figure 1 shows a sketch of a spanwise rotating channel. In addition to the dimensions of the channel, the flow is controlled by two non-dimensional numbers, i.e., the friction velocity based rotation number $Ro_\tau = 2\Omega\delta/u_\tau$ and the global friction Reynolds number $Re_\tau = u_\tau\delta/\nu$, where Ω is the rotation speed, δ is the half channel height, ν is the kinematic viscosity, and u_τ is the global friction velocity and is defined as $u_\tau = \sqrt{\delta f_x/\rho}$ with $f_x = -dP/dx$ being the driving body force and ρ being the fluid density. For a spanwise rotating channel, pressure at the two walls is different because of the Coriolis force, leading to a pressure side and a suction side. We can define friction velocities at the two walls, i.e., $u_{\tau,p}$ and $u_{\tau,s}$. The two friction velocities are not necessarily the same and they are related to the global friction velocity as $u_\tau = \sqrt{(u_{\tau,p}^2 + u_{\tau,s}^2)/2}$.

Johnston *et al.* (1972) showed that, for a channel that rotates about its spanwise axis at a reasonably high speed, the mean flow in the core region follows a linear scaling, i.e.,

$$U = 2\Omega y + C, \tag{1.1}$$

where C is a constant when given Ro_τ and Re_τ. Equation (1.1) is a counterpart of the

† Mechanical and Nuclear Engineering Department, Pennsylvania State University
‡ School of Aeronautics and Astronautics, Zhejiang University, China
¶ United Technologies Research Center
‖ Department of Aerospace Engineering, Mississippi State University
†† Department of Mechanical Engineering, Michigan State University

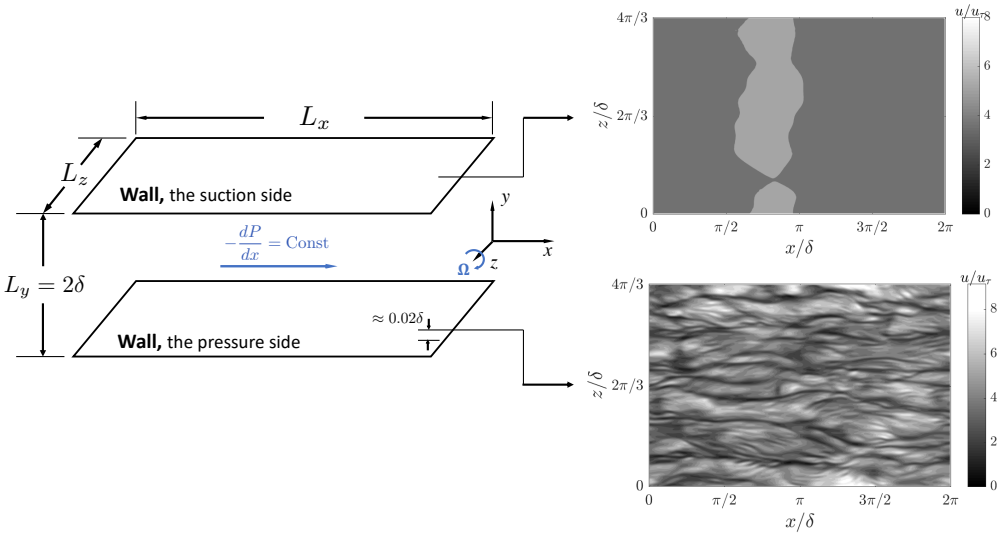

FIGURE 1. A sketch of flow in a spanwise rotating channel. Ω is the system rotation speed. x, y, and z are the streamwise, wall-normal, and spanwise directions, respectively. In a computational study, a periodic condition is often imposed in the streamwise direction. The domain size is $L_x \times L_y \times L_z$ in the streamwise, wall-normal, and the spanwise directions. δ is the half channel height. We also show contours of instantaneous streamwise velocities on two $x - z$ planes that are $y/\delta \approx 0.02$ from both walls. The flow near the pressure side remains turbulent, but the flow near the suction side is laminar. The flow is at a global friction Reynolds number $Re_\tau = 180$, and a friction rotation number $Ro_\tau = 20$, where u_τ is the global friction velocity. Details of the direct numerical simulation (DNS) can be found in Xia *et al.* (2016) and the references cited therein.

conventional universal logarithmic law of the wall, but because the function dependence of C on Ro_τ and Re_τ is not known, Eq. (1.1) does not have the same predictive power as the universal logarithmic law of the wall.

Since the early work of Johnston *et al.* (1972), flow in a spanwise rotating channel was extensively studied, including the experimental works by Nakabayashi & Kitoh (1996), Maciel *et al.* (2003) and Nakabayashi & Kitoh (2005), and the computational works by Kristoffersen & Andersson (1993), Yang & Wu (2012), Dai *et al.* (2016), and Hsieh & Biringen (2016). Some efforts were devoted to identifying the mean flow scaling. Here, we briefly review a few previous works. Nakabayashi & Kitoh (1996) conducted dimensional analysis and concluded that the mean velocity at a distance y from the pressure side is a function of the wall-unit-scaled distance from the wall $yu_{\tau,p}/\nu$, the friction Reynolds number Re_τ, and the Coriolis parameter $Rc = \Omega\nu/u_\tau^2 \equiv Ro_\tau/2Re_\tau$. The authors considered data at low rotation numbers ($Ro_\tau < 0.3$) and low Reynolds numbers ($Re_\tau < 310$) and argued that system rotation only adds a minor correction to the universal logarithmic law of the wall, where both κ and B may vary as Re_τ and Rc. Little was said about the scaling of the addend C in Eq. (1.1). Later, by analyzing the wind tunnel data from the University of Melbourne, Nickels & Joubert (2000) reported a rotation correction to the logarithmic law of the wall, i.e., $U^+ = 1/\kappa \ln y^+ + \beta Rc(y^+ - 35) + 5$, where, $\beta \approx 9.7$ is a constant. Again, nothing was said about the addend C in Eq. (1.1).

Although the mean flow may follow the revised logarithmic law of the wall in a wall-normal distance range, that range is limited. This is especially the case at high rotation

numbers. Hence, even by taking into account the additional terms, the conventional logarithmic law of the wall is often a poor approximation of the mean flow in a spanwise rotating channel (Brethouwer 2017), and the linear scaling in Eq. (1.1), which describes the mean flow scaling in a good extent of wall-normal distances, is a more useful scaling for rotating boundary-layer flows.

The objective of this work is to present a theoretical argument that leads to the universal scaling of the mean flow in spanwise rotating channels. The work focuses on the scaling of the addend C in Eq. (1.1), which contains the skin friction information. The mean flow scaling is compared to the available direct numerical simulation (DNS) data in the literature (Xia *et al.* 2016; Brethouwer 2017; Piomelli *et al.* 2018). The data cover a global Reynolds number range from $Re_\tau = 180$ to about $Re_\tau \approx 1500$ and a rotation number range from $Ro_\tau = 0$ to $Ro_\tau \approx Re_\tau$.

The rest of the paper is organized as follows: the mean flow scaling in Section 2; the theoretical argument that leads to this scaling in Section 3, a brief discussion of the results in Section 4; and concluding remarks in Section 5.

2. Mean flow scaling

The flow at the suction side is laminar-like at a reasonably high rotation number (see Figure 1). This work focuses on the flow at the pressure side. We define a rotation-induced length scale

$$l_\Omega = u_{\tau,p}/2\Omega. \tag{2.1}$$

By definition, $l_\Omega^+ \equiv l_\Omega/(\nu/u_{\tau,p}) = Re_{\tau,p}/Ro_{\tau,p}$. From a wall-normal distance $y = l_\Omega/\kappa$ to a distance $O(\delta)$ (we discuss why it is this range in Section 3), the mean flow at the pressure side follows Eq. (1.1), and the constant C is

$$C^+ \equiv \frac{C}{u_{\tau,p}} = \frac{1}{\kappa}\log(l_\Omega^+), \tag{2.2}$$

where + denotes normalization by the wall units at the pressure side.

Next, we compare Eq. (2.2) to data. Mean flow data are extensively available in the literature (Lamballais *et al.* 1996; Grundestam *et al.* 2008*a*; Yang & Wu 2012; Brethouwer 2017), and a number of data sets have been contributed by the authors of this work (Piomelli *et al.* 2018; Xia *et al.* 2016). In Figure 2 (a, b), we compare Eqs. (1.1) and (2.2) to data at $Re_\tau = 180$ and $Ro_\tau = 0$ to $Ro_\tau = 130$. For slowly rotating channels, the mean flow will not be very far from the conventional universal logarithmic law of the wall, and Eq. (1.1) applies to only a limited part of the flow. For rapidly rotating channels, the mean flow follows Eq. (2.2) in an extended wall-normal distance range from $y = l_\Omega/\kappa$ to a distance above which the flow is laminar. We compare Eq. (2.2) to DNS measurements in Figure 2 (c) for channel flows at $Re_\tau = 180$ and in Figure 2 (d) for channel flows at bulk Reynolds numbers Re_b from 5,000 to 31,600. Here, Re_b is the bulk Reynolds number defined based on the bulk velocity and the half channel height. The data lend strong support to the logarithmic scaling Eq. (2.2).

3. A mixing-length-type model

We present a mixing-length-type theoretical argument that leads to the mean flow scaling in Eqs. (1.1) and (2.2). First, we briefly review Prandtl's mixing length model.

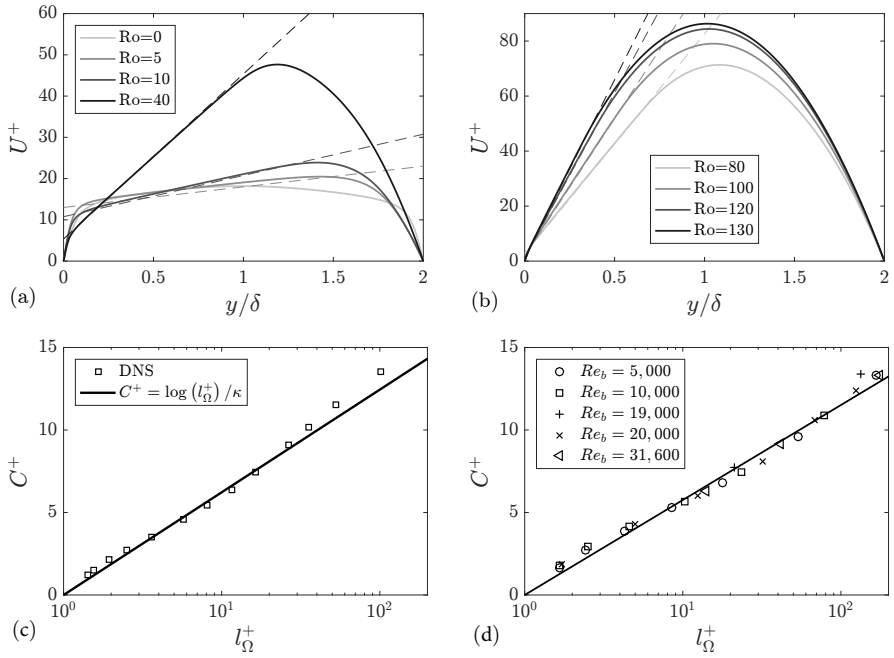

FIGURE 2. (a, b) Mean velocities in spanwise rotating channels. Flows are at a constant friction Reynolds number $Re_\tau = 180$. Normalization is by the global friction velocity u_τ and the half channel height, which are kept constant. The flow is laminar-like at the suction side (near $y/\delta = 2$). Equations (1.1) and (2.2) are shown using dashed lines. Details of the DNS are reported in Xia *et al.* (2016). (c, d) The constant C as a function of the rotation length scale l_Ω. Normalization is by wall units at the pressure side. Each data point represents one DNS calculation. (c) is for channel flow at $Re_\tau = 180$ and various rotation numbers. A $\kappa = 0.38$ is used. (d) is for flow at five bulk Reynolds numbers and different rotation numbers (Brethouwer 2017; Piomelli *et al.* 2018). A $\kappa = 0.33$ is used.

3.1. *Prandtl's mixing length hypothesis*

Prandtl's mixing length hypothesis is a classic model of high Reynolds number wall-bounded turbulence in non-rotating frames of reference (Prandtl 1925). We briefly review the mixing length model in this subsection. The mean flow equation for the streamwise momentum reads

$$\frac{d\langle UU\rangle}{dx} + \frac{d\langle UV\rangle}{dy} + \frac{d\langle UW\rangle}{dz} = \frac{d}{dy}\left[-\langle uv\rangle + \nu\frac{dU}{dy}\right] - \frac{1}{\rho}\frac{d\langle P\rangle}{dx}, \tag{3.1}$$

where we assume the flow is statistically stationary and the unsteady term is dropped. Prandtl argues that, at high Reynolds numbers, a constant stress layer emerges at wall-normal distances $\nu/u_\tau \ll y$, $y \ll \delta$, where the sum of the Reynolds stress and the viscous stress is a wall-distance-independent constant, i.e.,

$$-\langle uv\rangle + \nu\frac{dU}{dy} = \text{Const}, \tag{3.2}$$

where u, v are the velocity fluctuations in the streamwise and spanwise directions, respectively. In Eq. (3.2), we have dropped the pressure term and the mean convective terms. Integrating Eq. (3.1) from the wall to a distance $y = \epsilon \to 0$, we get $\text{Const} = \tau_w/\rho$. Per the mixing length hypothesis, the Reynolds stress may be modeled as the product of

an eddy viscosity, ν_T, and the mean velocity gradient, i.e., $-\langle uv\rangle = \nu_T dU/dy$. Prandtl proposed to model the eddy viscosity, ν_T, as the product of a mixing length, l_m, and the mean velocity gradient, i.e., $\nu_T = l_m^2 dU/dy$, where the mixing length may be thought of as the size of the eddies at the wall-normal distance y. For flat-plate boundary-layer flows with no system rotation, the mixing length is

$$l_m = \kappa y, \tag{3.3}$$

and the above arguments give rise to the well-known logarithmic law of the wall in a layer within which the viscous stress is negligible.

3.2. *A mixing length model for flow in spanwise rotating channels*

The mean flow in a spanwise rotating channel is uni-directional. Spanwise rotation leads to a mean Coriolis force in the wall-normal direction, which is balanced by pressure. The mean momentum equation is otherwise unchanged. Equation (3.1) is the mean flow equation for the streamwise momentum, and Eq. (3.2) is the equation for the streamwise momentum in the constant stress layer. In order to identify the law of the wall, we will need to model the Reynolds stress, and we do that by resorting to a mixing-length-type model.

Rotation forces the system at a scale l_Ω. This length scale competes with the scale of wall-attached eddies, i.e., κy. The result is a mixing length scale as shown in Figure 3(a), where the mixing length l_m increases as κy up to a wall-normal distance $y = l_\Omega/\kappa$, above which the mixing length stays a constant l_Ω, i.e.,

$$l_m = \min\left[\kappa y, l_\Omega\right], \quad l_\Omega = \frac{u_{\tau,p}}{2\Omega}. \tag{3.4}$$

The mixing length is a continuous function of y and therefore the transition occurs at $y = l_\Omega/\kappa$. Because spanwise rotating channel flow is a different flow than flat plate boundary layer flow, the constant κ is not necessarily equal to the classic value, 0.4.

Invoking the above mixing length model, above $y = l_\Omega/\kappa$, the mean flow equation becomes

$$\left(\frac{u_{\tau,p}}{2\Omega}\frac{dU}{dy}\right)^2 + \nu\frac{dU}{dy} = \tau_{w,p}/\rho \equiv u_{\tau,p}^2, \tag{3.5}$$

where the subscript p indicates quantities evaluated at the pressure side. At high Reynolds numbers and at distances away from the wall, where the viscous stress is negligible ($y\nu/u_{\tau,p} \gtrsim 30$), the mean flow equation becomes

$$\left(\frac{u_{\tau,p}}{2\Omega}\frac{dU}{dy}\right)^2 = u_{\tau,p}^2, \tag{3.6}$$

which gives rise to the linear scaling in Eq. (1.1). It is worth noting that the above arguments rely on a constant stress layer, which only exists at high Reynolds numbers.

In the earlier studies, there were few theories on the linear mean flow scaling, although many experiments and DNS confirmed its correctness (Lamballais *et al.* 1996; Nagano & Hattori 2003; Liu & Lu 2007; Grundestam *et al.* 2008*a*). Nakabayashi & Kitoh (1996) was able to get the linear scaling using dimension arguments, but the slope was determined by resorting to the experiment of Johnston *et al.* (1972) and the DNS of Kristoffersen & Andersson (1993). By studying the balance of the production and the Coriolis terms in the equation of $\langle uu\rangle$, Kristoffersen & Andersson (1993) and Grundestam *et al.* (2008*a*) also got the linear scaling. The mixing length model here adds on to the previous works and provides a new perspective on the mean flow scaling in the core region.

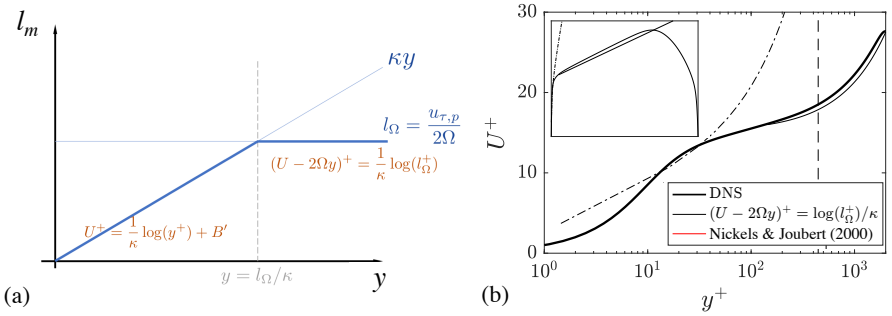

FIGURE 3. (a) Mixing length l_m in a spanwise rotating channel. l_m scales as κy up to a wall-normal distance $y = l_\Omega/\kappa$, above which the mixing length stays constant $l_m = l_\Omega$. (b) Mean flow in a rotating channel at a friction Reynolds number $Re_\tau = 1{,}213$ and a rotation number $Ro_\tau = 11.7$ (bold line) (Brethouwer 2017). Normalization is by the wall units at the pressure side. The thin solid line corresponds to the linear law of the wall, i.e., Eqs. (1.1) and (2.2), with $\kappa = 0.33$. The dashed line is at $y = l_\Omega/\kappa$. The revised logarithmic law of Nickels & Joubert (2000) is shown as the dash dotted line and is $U^+ = 1/\kappa \ln y^+ + \beta Rc(y^+ - 35) + 5$, where $\beta = 9.7$. The inset shows the mean velocity in a linear scale.

By requiring the mean velocity to be continuous at $y = l_\Omega/\kappa$ and the flow to be laminar at the limit of $l_\Omega^+ = 1$ (Grundestam *et al.* 2008*a*; Xia *et al.* 2016), we get the logarithmic scaling in Eq. (2.2). For flows at high Reynolds numbers and high rotation numbers, the mixing length model suggests a two-layer structure: the mean flow is logarithmic below $y = l_\Omega/\kappa$ and linear above. This is confirmed in Figure 3(b), thereby lending further support to the model. In Figure 3(b), we have also shown the revised logarithmic law of the wall in Nickels & Joubert (2000). Intended for flow in a slowly rotating reference frame (and therefore the comparison shown here is not a fair one), it is not unexpected that the revised logarithmic law does not capture the mean flow behavior.

3.3. *Extent of the linear layer and range of model applicability*

The linear layer emerges as the mixing length transitions from being proportional to the wall-normal distance to a constant. For a non-rotating channel, the mixing length is approximately κy up to a wall-normal distance $y/\delta \approx 0.2\delta$. In order for the above-mentioned transition to take place, the rotation-induced length scale must be such that $l_\Omega \lesssim 0.2\delta$, which leads to

$$5 \lesssim Ro_{\tau,p}. \tag{3.7}$$

The proposed mixing-length-type model is applicable only to rapidly rotating channels. Quantitatively, we consider $Ro_{\tau,p} \gtrsim 5$ as rapid rotation. The flow re-laminarizes for rotation numbers higher than $Ro_{\tau,p} = Ro_\tau \approx Re_\tau$ (the flow regains symmetry after it relaminarizes). Hence, the law of the wall, i.e., Eqs. (1.1) and (2.2), and the proposed mixing length model are relevant for flows such that $5 \lesssim Ro_{\tau,p}$, $Ro_{\tau,p} = Ro_\tau \lesssim Re_\tau$.

The mean flow is approximately linear and follows the linear law of the wall between $y_s = l_\Omega/\kappa$ and $y_e/\delta = 2 - u_{\tau,p}^2/u_\tau^2 + Ro_\tau/Re_\tau$, above which the flow is laminar-like (see detailed discussion in Xia *et al.* 2016). Figure 4 shows the mean profiles compensated by the logarithmic scaling. The profiles deviate from the logarithmic scaling at approximately $y_s = l_\Omega/\kappa$, as expected.

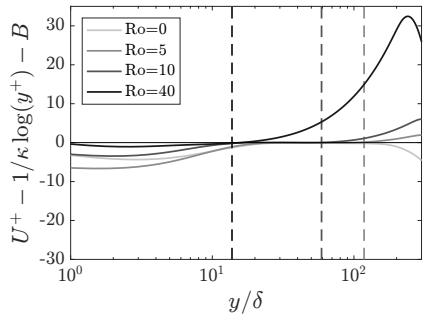

FIGURE 4. Mean profiles compensated by the near-wall logarithmic scaling. The data are the same as in Figure 2 (a). The dashed lines correspond to $y_s = l_\Omega/\kappa$ for each data set. At this Reynolds number, a logarithmic scaling cannot be found at a rotation number higher than 40.

4. Discussion

We briefly discuss the results and a few possible implications of the results.

4.1. *Wall modeling*

Knowledge of mean flow scaling can be leveraged for large-eddy simulation (LES) wall modeling. For wall-modeled LES, where the near-wall grid size scales with the local boundary-layer height, and the near-wall turbulence is not resolved by the coarse grid, the canonical no-slip condition no longer applies, and a wall model must be used to supply the LES equations with a proper wall boundary condition (Bose & Park 2018). LES wall modeling often invokes the law of the wall for directly relating the wall-shear stress to the near-wall LES velocity, or for turbulence parameterization within wall models (Yang *et al.* 2015, 2016*d*; Park & Moin 2014). The commonly used equilibrium wall model is such an example (Schumann 1975; Kawai & Larsson 2012). For flows in spanwise rotating channels, the conventional universal logarithmic law of the wall loses part of its predictive power, and Eqs. (1.1) and (2.2) must be employed. It follows that, for a rapidly rotating channel, with $l_\Omega/\kappa < \Delta$, the wall-shear stresses in a spanwise rotating channel can be modeled as

$$\tau_w/\rho = \left[\frac{\kappa(U - 2\Omega y)}{\log(l_\Omega^+)}\right]^2, \tag{4.1}$$

thereby reducing further modeling work needed for wall-modeled LES of spanwise rotating channel (e.g., the additional modeling used in Loppi *et al.* 2018). Here Δ is the grid spacing in the wall-normal direction. We test Eq. (4.1) by comparing the measured wall-shear stresses to the right-hand side of Eq. (4.1). Figure 5 shows the normalized wall-shear stress computed according to Eq. (4.1). The computed values are close to 1. In Figure 5, we have used flow information from flows at three rotation numbers and one bulk Reynolds number. Similar observations can be made at other Reynolds numbers and rotation numbers and for brevity are not shown here.

4.2. *A constant mixing length*

For flow in a spanwise rotating channel, rotation forces the system at a constant length scale l_Ω, leading to a constant mixing length. A constant mixing length was previously used to model the wake region (Pope 2001), where the flow is conventionally regarded as not being forced at any scale. While this is not directly relevant to this work, recent evidence shows that the above picture may need to be revised (Kwon 2016; Krug *et al.*

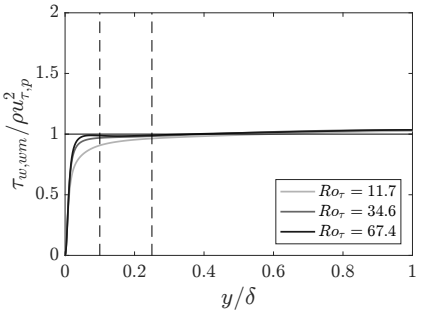

FIGURE 5. Wall-shear stresses computed according to Eq. (4.1). We use velocity information from flows at three rotation numbers $Ro_\tau = 11.7$, 34.6, 67.4 and one bulk Reynolds number $Re_b = 31{,}600$ (Brethouwer 2017). The two dashed lines are at $y/\delta = 0.1$, 0.25. For a typical wall-modeled LES, the first grid point locates at $y \approx O(0.1\delta)$ (Yang *et al.* 2017*b*), and the third grid point locates at $y \approx O(0.25\delta)$ (Kawai & Larsson 2012).

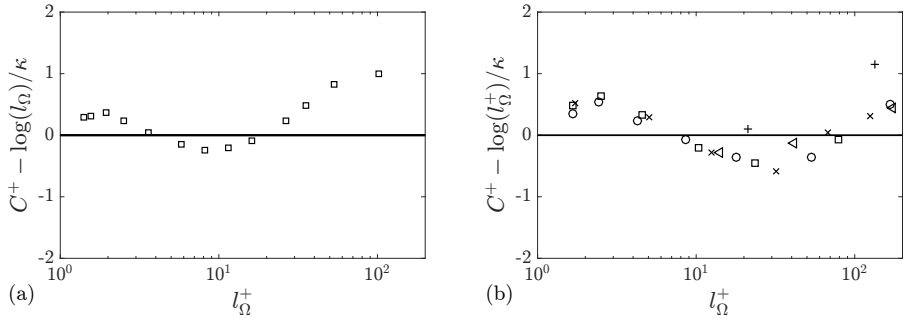

FIGURE 6. Compensated plots. The symbols in (a) are the same as in Figure 2 (c) and those in (b) are the same as in Figure 2 (d).

2017). Flow in wake regions is not fully turbulent but is at an intermittent state due to intrusions of the non-turbulent freestream in external flows and the quiescent core in internal flows (Xu & Yang 2018), which "forces" the flow in the wake at a constant length scale $O(\delta)$. This may be the physical mechanism behind a constant mixing length in non-rotating boundary-layer flows.

4.3. *Slowly rotating channels*

Equation 2.2 is obtained by requiring the mean flow to be continuous at $y = l_\Omega/\kappa$, below which the mixing length scales linearly with the distance from the wall, and above which the mixing length stays a constant. For slowly rotating channels, $l_\Omega = u_{\tau,p}/2\Omega$ is fairly large and $l_m \sim y$ may no longer be a good approximation of the mixing length. This leads to the observed deviations from Eq. (2.2) in Figure 2. For slowly rotating channels, the flow follows the universal logarithmic law of the wall near the wall and the law of the wake slightly away from the wall, before the mixing length abides the constant l_Ω and the mean flow exhibits a linear scaling. Because the wake is above the logarithmic law of the wall, deviations from the expected scaling Eq. (2.2) at small Ro_τ are expected to be positive. This expectation bears out in Figure 6, where we show the compensated plots of Figure 2 (c, d).

4.4. *Scales of fluid motions*

For flow in non-rotating reference frames, the sizes of the near-wall eddies scale as their distance from the wall leading to the mixing length in Eq. (3.3), which is the basic assumption of the Prandtl's mixing length model. A refinement of the Prandtl's mixing length model is Townsend's attached eddy hypothesis (Townsend 1976; Marusic & Monty 2019). By assuming that the eddy population density is inversely proportional to the wall-normal distance, i.e., $P(y) \sim 1/y$, the attached eddy hypothesis allows one to synthesize boundary-layer flows using randomly placed wall-attached eddies and extract scaling information from the synthesized flow fields (Perry & Marusic 1995; Marusic & Perry 1995). The attached eddy model has provided and probably will continue to provide useful insights into near-wall turbulence modeling in non-rotating reference frames (Yang et al. 2016a,c; 2017a) If the mixing lengths in Eq. (3.4) can be interpreted as the sizes of the near-wall eddies, i.e., if the near-wall eddies in a spanwise rotating channel scale as their distance from the wall up to $y = l_\Omega/\kappa$ and then stays constant, the attached eddy model can be re-cast to model turbulence in spanwise rotating channels. We only need to revise the eddy population density to $P(y) \sim \max[1/\kappa y, 1/l_\Omega]$, and we may use this model to estimate the scalings of flow statistics in spanwise rotating channels. For example, the logarithmic scaling of the streamwise velocity fluctuations was previously obtained by integrating the eddy population density from the location of interest to the boundary layer height, i.e., $\langle u^2 \rangle \sim \int_y^\delta P(y)dy \sim \log(\delta/y)$ (Yang *et al.* 2016*b*). It follows that the streamwise normal Reynolds stress in spanwise rotating channels is

$$\langle u^2 \rangle \sim \int_y^\delta P(y)dy \sim \int_y^\delta 1/l_\Omega dy \sim y, \tag{4.2}$$

leading to a linear scaling, which was previously reported in Xia *et al.* (2018). While this may be an interesting topic, we postpone further discussion on high-order statistics to future works, as the focus of this work is on the mean flow scaling.

5. Conclusions

We present a theoretical argument that leads to the mean flow scaling in spanwise rotating channels. The theoretical argument is a mixing-length-type model, where we model the rotation length scale and the scales of the conventional wall-attached eddies. The result is a mixing length that scales with the distance from the wall up to $y = l_\Omega/\kappa$ and then stays constant. By requiring velocity continuity and invoking the eddy viscosity, we get the linear law of the wall, i.e.,

$$(U - 2\Omega y)^+ = \frac{1}{\kappa}\log(l_\Omega^+),$$

where the superscript + normalization using wall units at the pressure side, κ is the Kármán constant, Ω is the rotation speed, and log is natrual log. The above mean flow scaling is compared to the available data in the literature, and the predicted logarithmic scaling was supported.

The predicted law of the wall is compared to two data sets, i.e., DNS in Xia *et al.* (2016) and Brethouwer (2017). The data seem to support a $\kappa \approx 0.38$ at low Reynolds numbers (Figure 2, c) and a $\kappa \approx 0.33$ at high Reynolds numbers. Recent measurements in high Reynolds number pipe and boundary layer flows suggest $\kappa = 0.4 \pm 0.02$. (Marusic *et al.* 2013; Bailey *et al.* 2014). Flow in a spanwise rotating channel is different from

that in a flat-plate boundary layer, and therefore we probably cannot expect the integral constant κ in a spanwise rotating channel to conform to the classic value. It is possible that κ in this flow depends on both Re and the Ro. But the fact that one κ collapses data from one paper and a different κ collapses data from the other paper, with both papers covering a good range of Reynolds numbers and rotation numbers, is calling for additional validation and verification. It is possible that the numerics, the domain size, or the resolution is responsible for the observed difference of κ between the two data sets, a topic left for future investigation.

In addition to validating the new law of the wall, we briefly discussed a few possible implications of the mean flow scaling. The mean flow scaling may be useful for LES wall modeling at high rotational speeds. We can also recast the attached eddy model according to the new mixing length. Last, it is worth mentioning that the identified mean flow scaling may also be relevant to Taylor-Couette flow (Grossmann *et al.* 2016), another topic left for future investigation.

Acknowledgements

X. Yang acknowledges the funding support to the CTR summer program, which made it possible for scientists from five different institutions to collaborate. Z.-H. Xia thanks S. Chen for many valuable comments and the financial support from the National Natural Science Foundation of China (Nos. 11772297 and 11822208). X.Y. thanks P. Moin and U. Piomelli for insightful comments and M.-W. Ge for editing the text. J. Yuan thanks U. Piomelli and W. Wu for sharing the high Reynolds number DNS data.

REFERENCES

Arolla, S. K. & Durbin, P. A. 2013 Modeling rotation and curvature effects within scalar eddy viscosity model framework. *Int. J. Heat Fluid Flow* **39**, 78–89.

Bailey, S., Vallikivi, M., Hultmark, M. & Smits, A. 2014 Estimating the value of Von Kármán's constant in turbulent pipe flow. *J. Fluid Mech.* **749**, 79–98.

Bose, S. T. & Park, G. I. 2018 Wall-modeled large-eddy simulation for complex turbulent flows. *Annu. Rev. Fluid Mech.* **50**.

Brethouwer, G. 2017 Statistics and structure of spanwise rotating turbulent channel flow at moderate Reynolds numbers. *J. Fluid Mech.* **828**, 424–458.

Choi, H. & Moin, P. 2012 Grid-point requirements for large eddy simulation: Chapman's estimates revisited. *Phys. Fluids* **24**, 011702.

Dai, Y.-J., Huang, W.-X. & Xu, C.-X. 2016 Effects of Taylor-Görtler vortices on turbulent flows in a spanwise-rotating channel. *Phys. Fluids* **28**, 115104.

Grossmann, S., Lohse, D. & Sun, C. 2016 High–Reynolds number Taylor-couette turbulence. *Anun. Rev. Fluid Mech.* **48**, 53–80.

Grundestam, O., Wallin, S. & Johansson, A. V. 2008*a* Direct numerical simulations of rotating turbulent channel flow. *J. Fluid Mech.* **598**, 177–199.

Grundestam, O., Wallin, S. & Johansson, A. V. 2008*b* A priori evaluations and least-squares optimizations of turbulence models for fully developed rotating turbulent channel flow. *Eur. J. Mech. B-Fluid* **27**, 75–95.

Hamba, F. 2006 The mechanism of zero mean absolute vorticity state in rotating channel flow. *Phys. Fluids* **18**, 125104.

Hsieh, A. & Biringen, S. 2016 The minimal flow unit in complex turbulent flows. *Phys. Fluids* **28**, 125102.

Hsieh, A. S., Biringen, S. & Kucala, A. 2016 Simulation of rotating channel flow with heat transfer: evaluation of closure models. *J. Turbomach.* **138**, 111009.

Johnston, J. P., Halleent, R. M. & Lezius, D. K. 1972 Effects of spanwise rotation on the structure of two-dimensional fully developed turbulent channel flow. *J. Fluid Mech.* **56**, 533–557.

Kawai, S. & Larsson, J. 2012 Wall-modeling in large eddy simulation: Length scales, grid resolution, and accuracy. *Phys. Fluids* **24**, 015105.

Kristoffersen, R. & Andersson, H. I. 1993 Direct simulations of low-Reynolds-number turbulent flow in a rotating channel. *J. Fluid Mech.* **256**, 163–197.

Krug, D., Philip, J. & Marusic, I. 2017 Revisiting the law of the wake in wall turbulence. *J. Fluid Mech.* **811**, 421–435.

Kwon, Y. 2016 The quiescent core of turbulent channel and pipe flows. PhD thesis, University of Melbourne.

Lamballais, E., Lesieur, M. & Métais, O. 1996 Effects of spanwise rotation on the vorticity stretching in transitional and turbulent channel flow. *Int. J. Heat Fluid Flow* **17**, 324–332.

Launder, B., Tselepidakis, D. & Younis, B. 1987 A second-moment closure study of rotating channel flow. *J. Fluid Mech.* **183**, 63–75.

Liu, N.-S. & Lu, X.-Y. 2007 Direct numerical simulation of spanwise rotating turbulent channel flow with heat transfer. *Int. J. Numer. Meth. Fl.* **53**, 1689–1706.

Loppi, N., Bodart, J. & Dufour, G. 2018 Wall-modeled large eddy simulation for rotating flows. In *Direct and Large-Eddy Simulation X*, pp. 263–269. Springer.

Maciel, Y., Picard, D., Yan, G., Gleyzes, C. & Dumas, G. 2003 Fully developed turbulent channel flow subject to system rotation. In *AIAA paper #2003-4153*, p. 4153.

Marusic, I. & Monty, J. P. 2019 Attached eddy model of wall turbulence. *Annu. Rev. Fluid Mech.* **0**.

Marusic, I., Monty, J. P., Hultmark, M. & Smits, A. J. 2013 On the logarithmic region in wall turbulence. *J. Fluid Mech.* **716**, R3.

Marusic, I. & Perry, A. 1995 A wall-wake model for the turbulence structure of boundary layers. Part 2. Further experimental support. *J. Fluid Mech.* **298**, 389–407.

Nagano, Y. & Hattori, H. 2003 Direct numerical simulation and modelling of spanwise rotating channel flow with heat transfer. *J. Turbul.* **4**, 8–8.

Nagib, H. M. & Chauhan, K. A. 2008 Variations of von Kármán coefficient in canonical flows. *Phys. Fluids* **20**, 101518.

Nakabayashi, K. & Kitoh, O. 1996 Low Reynolds number fully developed two-dimensional turbulent channel flow with system rotation. *J. Fluid Mech.* **315**, 1–29.

Nakabayashi, K. & Kitoh, O. 2005 Turbulence characteristics of two-dimensional channel flow with system rotation. *J. Fluid Mech.* **528**, 355–377.

Nickels, T. & Joubert, P. 2000 The mean velocity profile of turbulent boundary layers with system rotation. *J. Fluid Mech.* **408**, 323–345.

Park, G. I. & Moin, P. 2014 An improved dynamic non-equilibrium wall-model for large eddy simulation. *Phys. Fluids* **26**, 37–48.

Perry, A. & Marusic, I. 1995 A wall-wake model for the turbulence structure of

boundary layers. Part 1. Extension of the attached eddy hypothesis. *J. Fluid Mech.* **298**, 361–388.

Piomelli, U. & Balaras, E. 2002 Wall-layer models for large-eddy simulations. *Annu. Rev. Fluid Mech.* **34**, 349–374.

Piomelli, U., Wu, W. & J, Yuan 2018 Effect of roughness on wall-bounded flows subjected to spanwise rotation. In *ETMM11*. Leeds.

Pope, S. B. 2001 Turbulent flows. Cambridge Univ. Press.

Prandtl, L. 1925 Bericht uber untersuchungen zur ausgebildeten turbulenz. *Zs. angew. Math. Mech.* **5**, 136–139.

Schumann, U. 1975 Subgrid scale model for finite difference simulations of turbulent flows in plane channels and annuli. *J. Comput. Phys.* **18**, 376–404.

Smirnov, P. E. & Menter, F. R. 2009 Sensitization of the SST turbulence model to rotation and curvature by applying the Spalart–Shur correction term. *J. Turbul.* **131**, 041010.

Townsend, A. 1976 The structure of turbulent shear flow. *Cambridge Univ. Press, Cambridge* .

Von Kármán, T. 1930 Mechanische ahnlichkeit und turbulenz. *Math.-Phys. Klasse, pp. 58-76* .

Xia, Z., Brethouwer, G. & Chen, S. 2018 High-order moments of streamwise fluctuations in a turbulent channel flow with spanwise rotation. *Phys. Rev. Fluids* **3**, 022601.

Xia, Z., Shi, Y. & Chen, S. 2016 Direct numerical simulation of turbulent channel flow with spanwise rotation. *J. Fluid Mech.* **788**, 42–56.

Xu, H. H. & Yang, X. I. A. 2018 Fractality and the law of the wall. *Phys. Rev. E* **97**, 053110.

Yang, X. I. A., Baidya, R., Johnson, P., Marusic, I. & Meneveau, C. 2017*a* Structure function tensor scaling in the logarithmic region derived from the attached eddy model of wall-bounded turbulent flows. *Phys. Rev. Fluids* **2**, 064602.

Yang, X. I. A. & Lozano-Durán, A. 2017 A multifractal model for the momentum transfer process in wall-bounded flows. *J. Fluid Mech.* **824**.

Yang, X. I. A., Marusic, I. & Meneveau, C. 2016*a* Hierarchical random additive process and logarithmic scaling of generalized high order, two-point correlations in turbulent boundary layer flow. *Phys. Rev. Fluids* **1**, 024402.

Yang, X. I. A., Marusic, I. & Meneveau, C. 2016*b* Moment generating functions and scaling laws in the inertial layer of turbulent wall-bounded flows. *J. Fluid Mech.* **791**.

Yang, X. I. A. & Meneveau, C. 2016 Recycling inflow method for simulations of spatially evolving turbulent boundary layers over rough surfaces. *J. Turbul* **17**, 75–93.

Yang, X. I. A. & Meneveau, C. 2018 Hierarchical random additive model for wall-bounded flows at high Reynolds numbers. *Fluid Dyn. Res.* (In Press).

Yang, X. I. A., Meneveau, C., Marusic, I. & Biferale, L. 2016*c* Extended self-similarity in moment-generating-functions in wall-bounded turbulence at high Reynolds number. *Phys. Rev. Fluids* **1**, 044405.

Yang, X. I. A., Park, G. I. & Moin, P. 2017*b* Log-layer mismatch and modeling of the fluctuating wall stress in wall-modeled large-eddy simulations. *Phys. Rev. Fluids* **2**, 104601.

Yang, X. I. A., Sadique, J., Mittal, R. & Meneveau, C. 2015 Integral wall model for large eddy simulations of wall-bounded turbulent flows. *Phys. Fluids* **27**, 025112.

Yang, X. I. A., Sadique, J., Mittal, R. & Meneveau, C. 2016*d* Exponential roughness layer and analytical model for turbulent boundary layer flow over rectangular-prism roughness elements. *J. Fluid Mech.* **789**, 127–165.

Yang, Y.-T. & Wu, J.-Z. 2012 Channel turbulence with spanwise rotation studied using helical wave decomposition. *J. Fluid Mech.* **692**, 137–152.